Relation between information transfer and structure function in shell models

Jean-Luc Ottinger and Daniele Carati
Service de Physique Statistique, Plasma et Optique Non-Lineaire,
Faculté des Sciences, Université Libre de Bruxelles,
Campus Plaine, Code Postal 231, B-1050 Bruxelles, Belgium
(Received 7 September 1994; revised manuscript received 25 July 1995)

Shell models with conservation properties corresponding to two- and three-dimensional turbulence are presented together with other test models. Symmetry breaking in the information transfer between large and small scales is shown to be responsible for the convexity or the concavity of the scaling exponents of the structure function associated with intermittency corrections. The same effect is discussed in other models of intermittency.

PACS number(s): 47.27.−i

I. INTRODUCTION

For large Reynolds numbers, turbulence exhibits a well developed inertial range in which no characteristic length scale is observed. Dimensional analysis is then a powerful tool and had been used (together with simple assumptions on isotropic turbulence) more than 50 years ago by Kolmogorov [1] (K41) to derive the well known $k^{-5/3}$ law for the velocity spectrum. Although some of these assumptions have been criticized, the $k^{-5/3}$ law agrees extremely well with experimental data [2]. However, when higher-order quantities are considered, deviations from the Kolmogorov scaling are observed. A common example is given by the structure function of the longitudinal velocity increment $\delta_{\mathbf{r}}u(\mathbf{x},t) = u(\mathbf{x}+\mathbf{r},t) - u(\mathbf{x},t)$:

$$\langle [\delta_{\mathbf{r}}u(\mathbf{x},t)]^p \rangle \propto r^{\xi_p}. \tag{1}$$

Following Kolmogorov's phenomenology, the scaling exponents should grow linearly ($\xi_p = p/3$). Deviations from this simple law [3] are usually considered as a consequence and a proof of intermittency in the dissipation of energy. Although we agree with this argument, we consider the alternative point of view in which the deviations from the Kolmogorov scaling are related to the existence of a preferential direction for the transfer of information. In this paper, we systematically relate the information transfer between physical quantities to their two-time correlation. Indeed, when two variables $\mathcal{A}(t)$ and $\mathcal{B}(t)$ are coupled through a dynamic evolution equation, their two-time correlation

$$C_{\mathcal{AB}}(t,t') = \langle \mathcal{A}(t)\mathcal{B}(t') \rangle \tag{2}$$

is a measure of the information transfer ($\langle\,\rangle$ denotes the ensemble average). If $C_{\mathcal{AB}}(t,t')$ is larger for $t < t'$ than for $t > t'$, the influence of $\mathcal{A}$ on the future of $\mathcal{B}$ is more important than the influence of $\mathcal{B}$ on the future of $\mathcal{A}$. In that case, the dominant flux of information is from $\mathcal{A}$ to $\mathcal{B}$. This does not mean that other quantities (such as energy or enstrophy in the turbulent cascades) could not be transferred in the opposite direction.

Various models have been proposed to explain or to reproduce the deviations from the linear law ($\xi_p = p/3$). In some of them, such as the multifractal model [4,5] and the β models [6,7], the link with the Navier-Stokes (NS) equations more or less disappears. Their major advantage is to allow analytical calculations, which, in some cases (see the review [8]), are in good agreement with experimental data. More recently, She and Leveque [9] have proposed an improved intermittency model that keeps track of the NS dynamics by requiring the most singular structures to be filaments, in agreement with experimental and numerical observations. However, these models rely on time-independent arguments and on statistical properties of turbulence. The temporal evolution is roughly sketched, if not completely ignored, and these models are inherently restricted to spatial intermittency. Thus they are inadequate to show the relation between deviations from the Kolmogorov scaling and the existence of a preferential direction for the transfer of information. On the contrary, shell models [10–12] clearly appear as very convenient tools to investigate two-time correlations and transfer of information. Indeed, these models are low-dimensional dynamic systems in which the temporal evolution can be explicitly computed. Each dynamic variable $U_n(t)$ summarizes information from a shell of wave vectors and can be recorded for rather long periods by direct integration of the model. Thus, contrary to most of the other intermittency models, the shell models allow one to compute time series of some quantities. In Sec. II we introduce various shell models and we show in Sec. III how the information transfer might influence the function ξ_p. We also discuss how a preferential direction for information transfer is implicitly assumed in the intermittency models even when they are apparently time independent. In particular, we will show in Sec. IV that without this implicit assumption, the shape of the function ξ_p would be very different. Finally, the results are summarized in Sec. V and a discussion is presented on the possible importance of the existence of a preferential direction for information transfer in turbulence modeling.

II. SHELL MODELS

Although the shell models cannot be derived directly from the NS equations, they have been developed to reproduce as correctly as possible the NS dynamics. Thus it is usual to describe the shell models by stressing the analogy with the NS equations. The Fourier space is divided into shells centered on the origin and including the wave vectors $\mathbf{k}$ such as $k_0 g^{n-1/2} \leq |\mathbf{k}| < k_0 g^{n+1/2}$. The typical norm of wave vectors in shell n thus follows a geometrical progression $k_n = k_0 g^n$. Here k_0 represents some characteristic norm and we adopt the usual choice $g = 2$. All the information from velocity Fourier modes with $\mathbf{k}$ in the shell n is then summarized by a single complex variable U_n. The equations governing the evolution of the U_n are then supposed to reproduce the basic ingredients of turbulence, i.e., local and conservative bilinear interactions (proportional to k), molecular dissipation (proportional to k^2) and external forcing acting in the small wave vectors range:

$$\partial_t U_n = f_n - \nu k_n^2 U_n + i(\alpha\, k_{n+1}\, U_{n+1}^*\, U_{n+2}^* + \beta\, k_n\, U_{n+1}^*\, U_{n-1}^* + \gamma\, k_{n-1}\, U_{n-1}^*\, U_{n-2}^*), \quad (3)$$

where f_n and $\nu k_n^2 U_n$ are, respectively, the forcing and dissipation terms. In order to mimic the locality of mode interaction, the shell variable U_n is only coupled to U_{n-2}, U_{n-1}, U_{n+1}, and U_{n+2}. It has been noted that any choice of the interaction coefficients $\{\alpha, \beta, \gamma\}$ defines a specific shell model for which the nonlinear interaction conserves two quantities. In particular, when the solutions of the equation

$$\alpha + \beta g^\lambda + \gamma g^{2\lambda} = 0 \quad (4)$$

correspond to real and positive values of g^λ, the shell model conserves the quantity $Q_\lambda = \sum_n |U_n|^2 k_n^\lambda$ [13]. When shell models are used to reproduce the statistical properties of turbulence, it is natural to impose energy conservation, i.e., conservation of $E = Q_0$. In that case, $\alpha+\beta+\gamma = 0$ and we may define $\{\alpha, \beta, \gamma\} = p\{1, \epsilon, -1+\epsilon\}$. The parameter p can always be included in the definition of t, f, and ν. Thus, when energy conservation is imposed, only ϵ influences the properties of the model. However, this influence is important. For example, it has been observed [14] that for $\epsilon \lesssim 0.3843$, the system is stable while it becomes chaotic for $\epsilon \gtrsim 0.398$. Most of the authors [10,11,14,15] considering the three-dimensional case have used $\epsilon = 1/2$. In that case the second solution of Eq. (4) is $g^\lambda = -2$ and corresponds to the conservation of $H = \sum(-g)^n |U_n|^2$. Recently [13], this choice ($\epsilon = 1/2$) has been justified by noting that it corresponds to the conservation of helicity in the original NS equation. This particular value of ϵ also leads to the best agreement between shell models and experimental data. For all these reasons, we adopt $\epsilon = 1/2$ for modeling the three-dimensional (3D) turbulence and we denote M3 the corresponding shell model.

The two-dimensional (2D) shell model M2 is fully determined by the conservation of both energy and enstrophy $Z = Q_2$ ($\{2, -5/2, 1/2\}$, $\epsilon = 5/4$). The use of M2 is less frequent that M3 mainly because the cascade picture of 2D turbulence is more questionable. A recent approach [16] shows that the behavior of a slightly modified shell model may be understood using formal nonequilibrium statistical mechanics close to local equilibrium. The observed fluxes of the conserved quantities are then explained by simple diffusion due to the gradients of conjugate quantities of Q_2 and Q_0 instead of cascade processes. However, the shell model used here does not seem to lead directly to the same conclusion and we have not found any convincing argument to distinguish definitely between the local equilibrium and the cascade picture of 2D shell models.

Finally, we also introduce two test models: Ma, for which the conserved quantities are Q_4 and Q_0 ($\{2, -17/8, 1/8\}$, i.e., $\epsilon = 17/16$), and Mb, for which the roots of Eq. (4) coincide so that only one quantity is conserved ($\lambda = 4$). For Mb, the use of the notation ϵ is meaningless since energy is not conserved ($\{2, -1/4, 1/128\}$). The choice of these models is motivated in Sec. III by the dynamic behavior of the shell variables.

The forcing f_n used here is a random Gaussian noise acting on modes 2 and 3 and for which we can choose the

TABLE I. Main characteristics of the shell models used in this paper.

Characteristic	M3	M2	Ma	Mb
coefficients $\{\alpha, \beta, \gamma\}$	$\{2, -1, -1\}$	$\{2, -5/2, 1/2\}$	$\{2, -17/8, 1/8\}$	$\{2, -1/4, 1/128\}$
conserved quantities	Q_0, H	Q_0, Q_2	Q_0, Q_4	Q_4
number of shells N	19	21	20	20
k_0	1/8	1/4	1/4	1/4
injection rate	Q_0 ($\bar{\epsilon} = 4 \times 10^{-4}$)	Q_2 ($\bar{\eta} = 0.12$)	Q_4 ($\bar{\zeta} = 6.0$)	Q_4 ($\bar{\zeta} = 4.0$)
viscosity ν	10^{-6}	6×10^{-12}	10^{-14}	5×10^{-14}
U_1 damping	no	$-10U_1$	$-0.05U_1$	$-0.05U_1$
k_{diss}	$\left(\bar{\epsilon}/\nu^3\right)^{1/4} \approx k_{16}$	$\left(\bar{\eta}/\nu^3\right)^{1/6} \approx k_{20}$	$\left(\bar{\zeta}/\nu^3\right)^{1/8} \approx k_{19}$	$\left(\bar{\zeta}/\nu^3\right)^{1/8} \approx k_{19}$
scaling law $U_n^p \propto k_n^{-\mu p}$; μ	1/3	1	5/3	5/3
scaling law $t_c(n) \propto k_n^\rho$; ρ	$-2/3$	0	2/3	2/3
inertial range (IR)	4–15	6–16	8–16	9–16
turnover times in the IR	4700 − 51000	$2.7 \times 10^5 - 1.5 \times 10^5$	$9.1 \times 10^5 - 2900$	$6.4 \times 10^5 - 14000$

injection rate of the conserved quantity (for instance, $\bar{\epsilon}$, the energy injection rate for M3). A comparison with a deterministic forcing with the same injection rate does not show any major difference. In M2, Ma, and Mb simulations, we add a "large-scale damping" to avoid any piling up of energy in the first shell. The definitions of all the parameters entering in these shell models are summarized in Table I.

The numerical simulations of shell models do not directly give the structure function associated to the longitudinal velocity increments (1). However, equivalent information can be obtained by computing higher moments of the shell variables. Indeed, each U_n is a measure of the velocity change over length scales of the order of k_n^{-1}. Thus they play the same role as the velocity increments. It is then usually considered that the exponents ξ_p in

$$\langle |U_n|^p \rangle \propto k_n^{-\xi_p} \tag{5}$$

are the same as the exponents appearing in the quantities (1). This is the traditional way shell models have been used to explore intermittency corrections to the Kolmogorov scaling. The information given by (5) is related to the spatial intermittency of the velocity field.

III. INFORMATION TRANSFER AND STRUCTURE FUNCTION IN SHELL MODELS

Shell models give a simplified picture of turbulence by drastically reducing the spatial description of the system. Indeed, the complete space is reduced to a small set of points related to shells. However, the temporal evolution is described by a continuous variable and provides detailed information regarding dynamic behaviors. This interesting property has already been exploited [10,11] for computing the Lyapunov exponents associated with the shell variables dynamics. Here we focus on quantities that are related to the two-time correlation between neighbor shells. It will be convenient to present the results in terms of the real variables ρ_n introduced in Ref. [15]:

$$\rho_n(t) e^{i\theta_n} = {k_n}^{\mu} U_n(t), \tag{6}$$

where μ is chosen such that $\rho_n \propto 1$ by using dimensional analysis based on Kolmogorov-type arguments. This exponent depends on the model ($\mu = 1/3$ for M3 and $\mu = 1$ for M2; see Table I). The solution $\rho_n = 1\ \forall n$ is the fixed point of the unforced, inviscid shell model and leads to the "Kolmogorov" linear law $\xi_p = \mu p$. We now introduce the centered and normalized two-time correlations for the ρ_n

$$C_{n,n'}(\tau) = \frac{\langle \rho_n(t)\rho_{n'}(t+\tau t_n^c)\rangle - \langle \rho_n\rangle\langle \rho_{n'}\rangle}{\sqrt{\langle \rho_n^2\rangle - \langle \rho_n\rangle^2}\sqrt{\langle \rho_{n'}^2\rangle - \langle \rho_{n'}\rangle^2}}, \tag{7}$$

where $\langle\ \rangle$ denotes the time average. In practice, averages are evaluated over a large number of turnover times of the slowest variable (see Table I). As discussed in the Introduction, the quantities (7) are related to the information transfer between shell variables. If the maximum of $C_{n,n'}(\tau)$ is achieved for $\tau = \tau^*_{n,n'} > 0$ (< 0), the model is considered to experience a *direct* (*inverse*) transfer of information from variable n to variable n'. By definition, these two-time correlations have the following properties: $C_{n,n}(0) = 1$ and $C_{n',n}(\tau) = C_{n,n'}(-\tau)$. Moreover, the asymptotic value of these correlations vanishes [$C_{n,n'}(\tau) \to 0$ for $\tau \to \infty$]. Indeed, for large τ, ρ_n and $\rho_{n'}$ are independent quantities and $\langle \rho_n(t)\rho_{n'}(t+\tau t_n^c)\rangle$ may be approximated by $\langle \rho_n\rangle\langle \rho_{n'}\rangle$ so that the numerator in (7) vanishes. Here τ is a dimensionless quantity that measures the delay between the arguments of variables ρ_n and $\rho_{n'}$ in (7) in terms of the characteristic time t_n^c of shell n defined by

$$t_n^c = \left\langle \frac{\rho_n(t)}{\dot{\rho}_n(t)} \right\rangle. \tag{8}$$

A simple dimensional analysis provides a rough estimate for these characteristic times $t_n^c \propto k_n^{\mu-1}$, which is reasonably well fitted by the numerical results (Fig. 1). Our

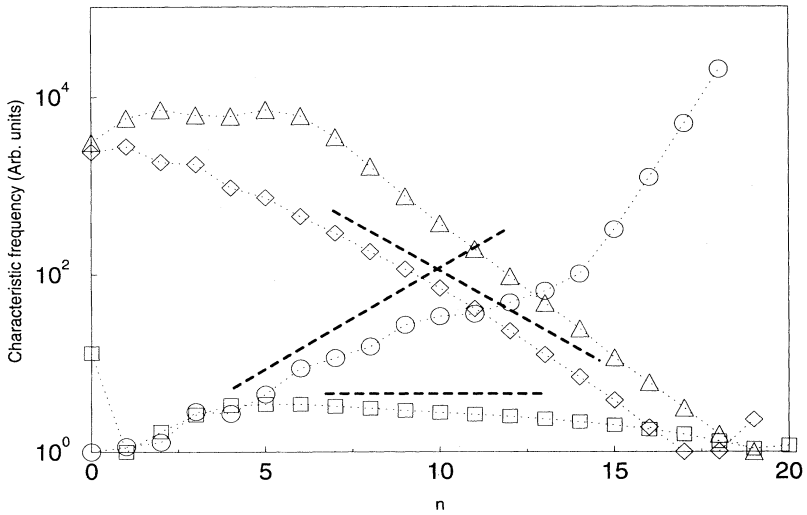

FIG. 1. Logarithmic plot of the measured characteristic frequencies τ_n^{-1} (normalized by the smallest one) for M3, ○; M2, □; Ma, △; and Mb, ◇. The dashed lines correspond to the Kolmogorov-like analysis.

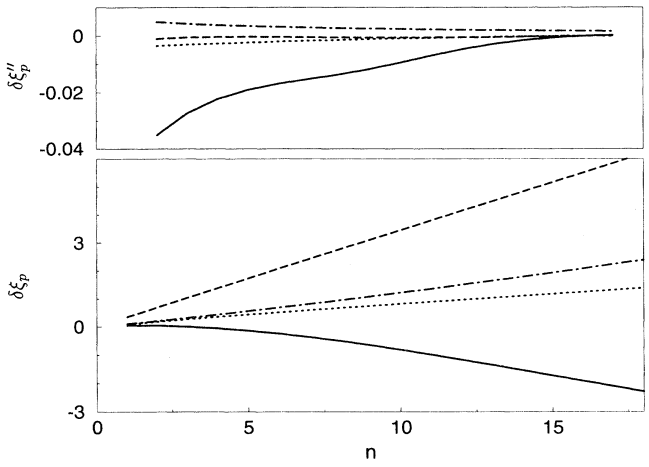

FIG. 2. Deviations $\delta\xi_p = \xi_p - \mu\ p$ from the Kolmogorov scaling are presented for M3 (——), M2 (·····), Ma (— — —), and Mb (·—·—·) in the lower part of the figure. The upper part of the figure shows the "discrete second derivative" $(\delta\xi_{p+1} - \delta\xi_p) - (\delta\xi_p - \delta\xi_{p-1})$ of the ξ_n. The M3 and M2 curves are convex, the Ma curve is almost linear, and the Mb curve is concave.

choice for the models Ma and Mb is motivated by the particular scaling of their characteristic times ($t_n^c \propto k_n^{2/3}$), which is the opposite scaling of M3 (proportional to $k_n^{-2/3}$). Fast (slow) variables in M3 should thus correspond to slow (fast) variables in Ma and Mb.

For each model, we have computed the ξ_p by using the method proposed by Kadanoff *et al.* [13], which eliminates the period three oscillations in the spectra (Fig. 2). In order to distinguish between convex and concave ξ_p, we have shown on the same figure the discrete second derivative of the function $\xi_p'' = (\xi_{p+1} - \xi_p) - (\xi_p - \xi_{p-1})$.

A. M3

The simulation of M3 shows a well developed inertial range determined by a constant energy flux. The scaling exponents ξ_p exhibit the expected convex deviations to the K41 scaling. We present the two-time correlations $C_{n,n}$, $C_{n,n+1}, \ldots, C_{n,n+3}$ in Fig. 3 for $n = 10$. The long-time behavior of these functions does not allow an accurate determination of the decay exponents ϕ $[C_{n,n+1}(\tau) \propto \tau^{-\phi}]$. However, we can compare this decay with the theoretical prediction of Kadanoff *et al.* [13]. By using the relations (Legendre transforms) derived in this reference between the decay exponents and the ξ_n, we have obtained $\phi \sim 0.047$. The decay we have numerically observed would clearly correspond to a much higher value of ϕ. The long-time shapes of the $C_{n,n+p}$ look independent of p. In the embedded figure we focus on the short-time behavior. The maximal value of the correlation $C_{n,n+p}$ is achieved after a delay $\tau^*_{n,n+p}$. These delays are plotted for various n in Fig. 4. They are always positive. The energy cascade in 3D turbulence is thus associated with a dominant direct transfer of information. This observation is in agreement with the commonly accepted picture of a dominant influence from slow to fast variables. One also observes the ordering

$$\tau^*_{n,n+3} > \tau^*_{n,n+2} > \tau^*_{n,n+1} > 0. \tag{9}$$

In the inertial range, the dimensionless time delays should be constant ($\tau^*_{n,n+i} = \tau_i$) since they are nor-

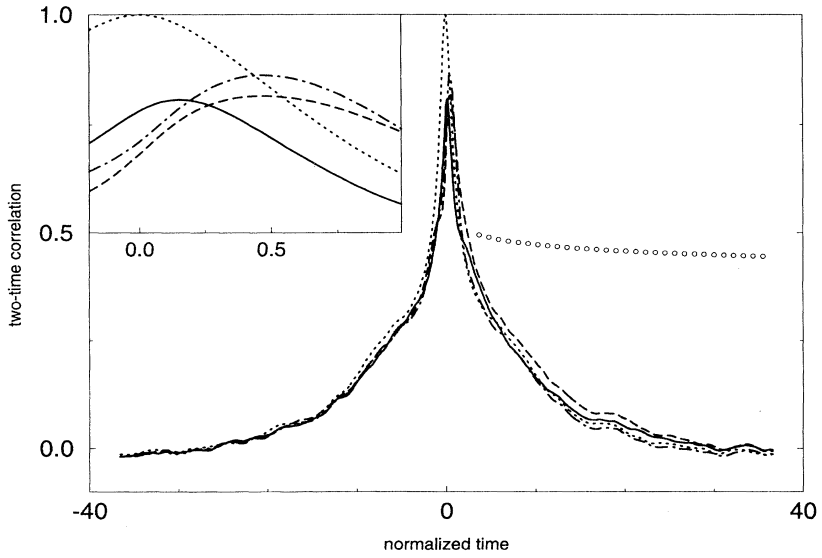

FIG. 3. Time correlations $C_{n,n+p}(\tau)$ for $n = 10$ and $p = 0$, 1, 2, and 3 (dotted, solid, dashed, and dot-dashed lines, respectively) for M3. The circles show a decaying function proportional to $\tau^{-0.047}$ as predicted by Benzi *et al.* In the inset the correlations are shown in the region around $\tau = 0$ with the same vertical scale. The maximal values of the correlations $p \neq 0$ are achieved after a positive delay $\tau^*_{n,n+p}$.

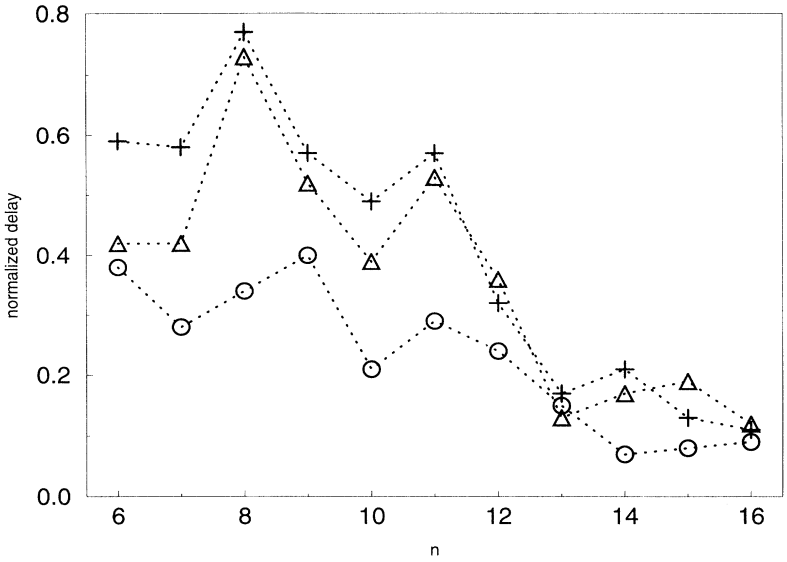

FIG. 4. Normalized time delays $\tau^*_{n,n+p}$, $p = 1, \circ$; $p = 2$, $\triangle$; $p = 3$, $+$, needed to reach the maximal value of the correlation $C_{n,n+p}$.

malized by the appropriate t^c_n. Actual measurements show a weak n dependence in $\tau^*_{n,n+i}$, which might be due to sampling limits. A good estimate for τ_i is then obtained by averaging the $\tau^*_{n,n+i}$ over n in the inertial range ($n \in [6,12]$) $\bar{\tau}_i = \langle \tau^*_{n,n+i} \rangle_n$. The values obtained for $\bar{\tau}_1$, $\bar{\tau}_2$, and $\bar{\tau}_3$ suggest that the cascade is essentially dominated by first neighbor interactions. Indeed, the real time needed to reach the maximal value of $C_{n,n+2}$ is $\bar{\tau}_2 t^c_n$. It is well approximated by the sum of the real times needed to reach the maximal values of, respectively, $C_{n,n+1}$ (i.e., $\bar{\tau}_1 t^c_n$) and $C_{n+1,n+2}$ (i.e., $\bar{\tau}_1 t^c_{n+1}$). Indeed, we have measured that $\bar{\tau}_2 t^c_n \sim \bar{\tau}_1 t^c_n + \bar{\tau}_1 t^c_{n+1}$ or, equivalently, $\bar{\tau}_2 \sim \bar{\tau}_1 (1 + g^{-2/3})$. Analogously, we have measured that $\bar{\tau}_3 \sim \bar{\tau}_1 (1 + g^{-2/3} + g^{-4/3})$, supporting again the picture of dominant first neighbor interactions. Quantitatively, we have

$$\begin{aligned} &\bar{\tau}_1 = 0.29 \ , \\ &\bar{\tau}_2 = 0.49 = 1.69\ \bar{\tau}_1 \approx \bar{\tau}_1\ (1 + g^{-2/3}) = 1.63\ \bar{\tau}_1 \ , \\ &\bar{\tau}_3 = 0.56 = 1.93\ \bar{\tau}_1 \approx \bar{\tau}_1\ (1 + g^{-2/3} + g^{-4/3}) = 2.02\ \bar{\tau}_1 \ . \end{aligned} \tag{10}$$

This corresponds to the usually accepted phenomenology of the inertial range (dominated by local interactions) even if the shell variables U_n are directly coupled to both $U_{n\pm1}$ and $U_{n\pm2}$. We also note that the third-neighbor correlation does not seem to be influenced by the observed period-three oscillations in the spectra and $C_{n,n+3}$ looks similar to the other correlations.

Because of the interest of the multipliers introduced by Benzi *et al.* [15] for the 3D case (see Sec. IV), we have also studied the quantities

$$a_n(t) = \rho_{n+1}(t)/\rho_n(t) \tag{11}$$

and their two-time generalizations

$$b_n(t',t) = \rho_{n+1}(t')/\rho_n(t). \tag{12}$$

Here we have computed the two-time correlations

$$A_{n,n'}(\tau) = \frac{\langle a_n(t) a_{n'}(t + \tau t^c_n) \rangle - \langle a_n \rangle \langle a_{n'} \rangle}{\sqrt{\langle a_n^2 \rangle - \langle a_n \rangle^2} \sqrt{\langle a_{n'}^2 \rangle - \langle a_{n'} \rangle^2}} \tag{13}$$

and the averaged two-time multipliers

$$\bar{b}_n(\tau) = \langle b_n(t + \tau t^c_n, t) \rangle. \tag{14}$$

The t dependence disappears because of the time averaging. The results are presented in Fig. 5. Again, we observe that these quantities are not centered on $\tau = 0$ (except of course for $A_{n,n}$). It is thus interesting to note that the measurements presented in Ref. [15] for the verification of the independence of the multipliers, which are equivalent to our $A_{n,n+p}(0)$, did not correspond to the highest correlation between the considered quantities. Fortunately, even at their maximal value, the correlation remains small enough to justify the approximation of statistical independence between the different a_n. We also note that the correlations $A_{n,n'}(\tau)$ vanish much faster than the correlations $C_{n,n'}(\tau)$. This is probably due to the fact that the variables ρ_n entering the quantity $C_{n,n'}$ account for slow variations of the spectrum amplitude around its equilibrium value while the ratios a_n in $A_{n,n'}$ only measure deviations from the local slope of the spectrum. Clearly, the amplitude of the spectrum varies on time scales much longer than the local and instantaneous value of the characteristic exponent. Following this point of view, the ρ_n and their correlations are more suitable for describing bursts of energy and the mechanism of charge and discharge in the model than the variables $a(t)$.

Finally, we note that the discrepancy between the observed t^c_n and the dimensional analysis prediction $k_n^{\mu-1}$ is more important for M3 than for the other models (Fig. 1). One might interpret this effect as a consequence of the dominating transfer of information coming from the slow variables, which could slow down the cascade process in

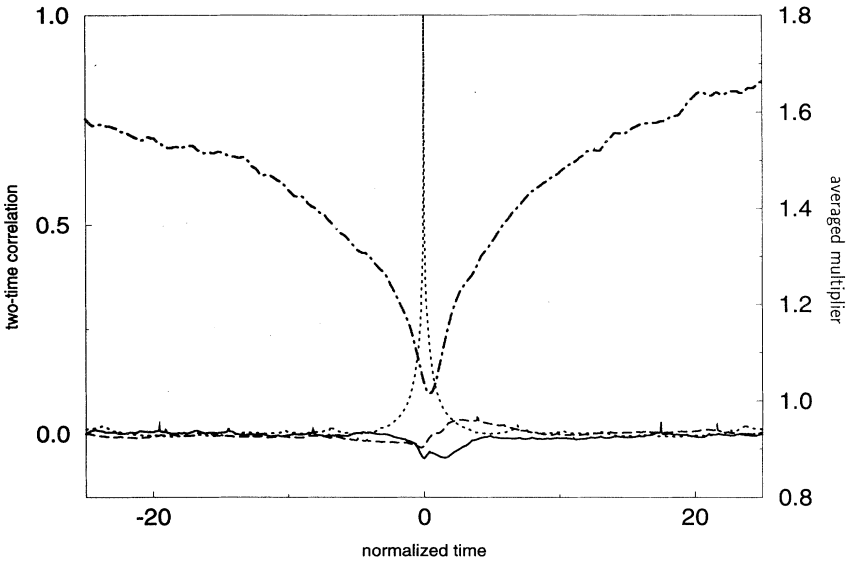

FIG. 5. Averaged two-time multiplier $\bar{b}_{10}(\tau)$ (dot-dashed curve, right axis) and the two-time correlations $A_{n,n+p}(\tau)$, $n = 10$ and $p = 0$, 1, and 2 (dotted, solid, and dashed curves, respectively) of the multipliers $a_n(t)$ in the case M3. The extremal values are not achieved at $\tau = 0$.

the high k range. However, we do not have specific measurements to quantify and to support this possible effect.

B. M2

The simulation of M2 shows an inertial range with constant enstrophy flux and without energy flux in agreement with theoretical arguments [17]. The deviations from the dimensional analysis are weak and slightly convex (see Fig. 2). The correlations $C_{n,n+p}(\tau)$ are plotted in Fig. 6 for $n = 12$ and $p = 0, 1, 2, 3$. The correlation $p = 1$ exhibits clear and simultaneous direct and reverse transfers of information in contrast with the strongly dominant direct information transfer in M3. For the variable U_n, the maxima of the two-time correlation correspond to two different phenomena: reception of information from U_{n+1} (peak at $\tau \approx -1.9$) and transmission of information to U_{n+1} (peak at $\tau \approx +1.9$). However, since the maximum corresponding to $\tau \approx +1.9$ is higher, the dynamics seems to be slightly dominated by direct transfer of information. The correlations $p = 2$ and $p = 3$ exhibit also a disymmetry supporting the dominance of the forward transfer, but do not seem to be related to the first-neighbor correlation like in M3. If it were the case, we could expect to have a higher positive peak for the second-neighbor correlation at $\tau \sim 0$, resulting from the combination of forward and backward exchanges of in-

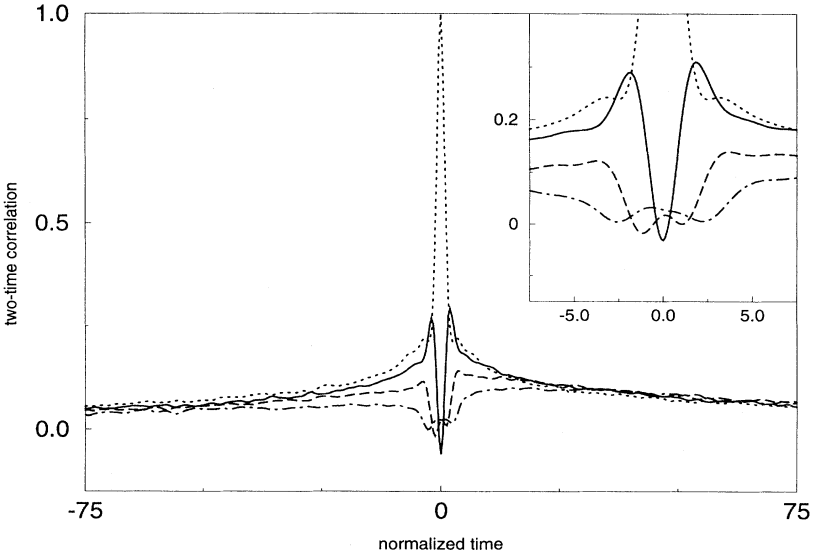

FIG. 6. Time correlations $C_{n,n+p}(\tau)$ for $n = 12$ and $p = 0$, 1, 2, and 3 (dotted, solid, dashed, and dot-dashed lines, respectively) for the M2 model. The two peaks in $C_{n,n+1}$ correspond to direct and reverse transfers of information. The direct transfer is dominant. This figure is restricted to the range $\tau \in [-75, 75]$ for the sake of clarity. Within this range it is not clear that $C_{n,n+p}(\tau)$ vanishes for large τ. However, this theoretical prediction has been numerically checked by extending the measurement to $\tau \approx 300$.

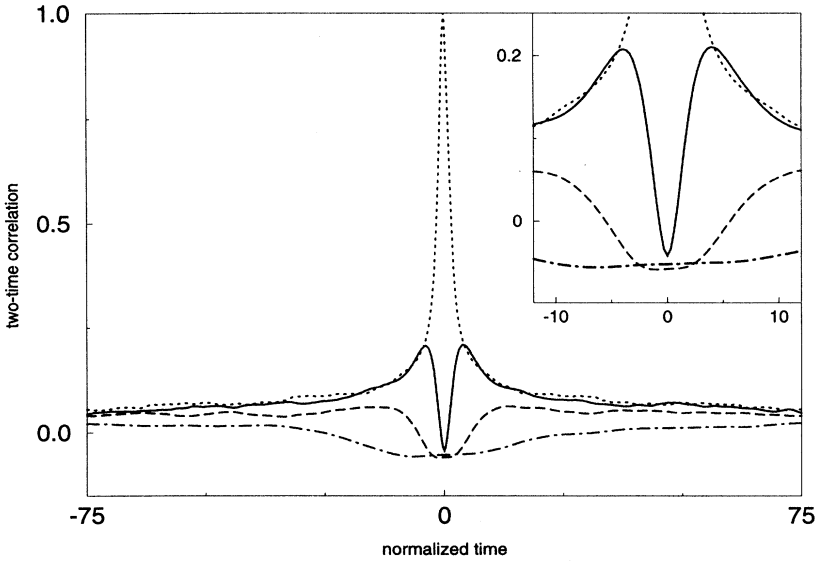

FIG. 7. Time correlations $C_{n,n+p}(\tau)$ for $n = 10$ and $p = 0$, 1, 2, and 3 (dotted, solid, dashed, and dot-dashed lines, respectively) for Ma. The two peaks in $C_{n,n+1}$ correspond to direct and reverse transfers of information.

formation with variable $n+1$. Thus, contrary to M3, M2 does not seem to be dominated by first-neighbor interactions. We note that shell models for two-dimensional turbulence are sometimes criticized because nonlocal interactions could be important in two dimensions. Here we see that M2 seems to develop nonlocal interactions, while it has been constructed using local coupling only.

C. Ma and Mb

Simulations of Ma and Mb also show an inertial range with a constant flux of Q_4. The scaling exponents of the structure functions, shown in Fig. 2, exhibit deviations from the Kolmogorov-like prediction $\xi_p = 5/3p$: slopes at the beginning of the curves are given by $\xi_1 = 2.01$ for Ma and $\xi_1 = 1.77$ for Mb. Thus energy conservation in Ma strongly modifies the slope of the spectra, even if the energy flux vanishes in the Q_4 cascade. The correlation functions of Ma and Mb are presented in Figs. 7 and 8 for $n = 10$ and $n = 12$. Their structure are similar to the M2 case. The information transfers are similar in both directions in the Ma case. It is interesting to note that the reverse information transfer dominates in the Mb case, while there is no reverse cascade in this model. We thus conclude that the information transfers are not directly related to the transport of the conserved quantities.

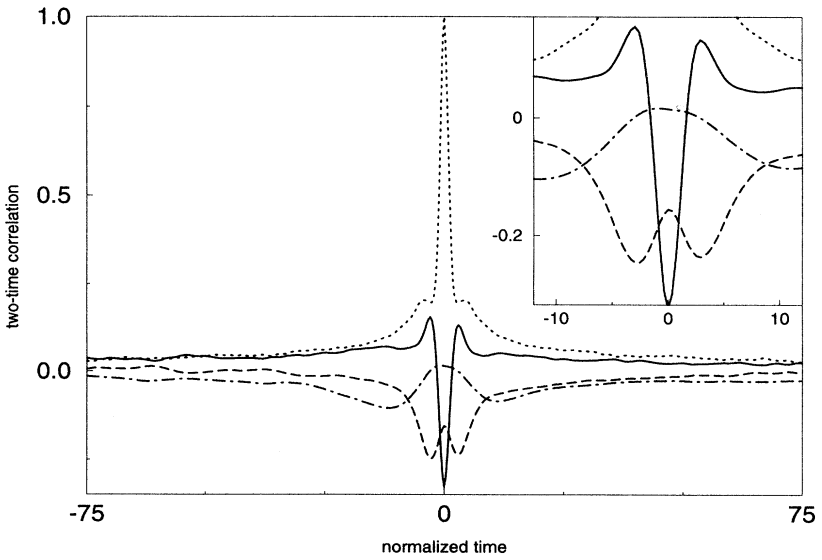

FIG. 8. Time correlations $C_{n,n+p}(\tau)$ for $n = 12$ and $p = 0$, 1, 2, and 3 (dotted, solid, dashed, and dot-dashed lines, respectively) for the Mb model. The two peaks in $C_{n,n+1}$ correspond to direct and reverse (and dominant) transfers of information.

We also note for Ma and Mb that the correlation $C_{n,n+p}(\tau = 0)$ is negative for $p \neq 0$. Thus values of ρ_n larger (smaller) than $\langle \rho_n \rangle$ are preferentially observed together with values of ρ_{n+p} smaller (larger) than $\langle \rho_{n+p} \rangle$. Physically, this corresponds to a return to the average spectrum by an exchange of energy between neighbor shells. This effect is also observed for M2 and is totally different from the M3 case for which the positive correlation $C_{n,n+p}(\tau = 0)$ for $p \neq 0$ might be interpreted as a return to the average spectrum by a collective variation of several neighbor shell variables.

D. Transfer of information and convexity of the ξ_n

By analyzing these four models, we have shown that their dynamics are characterized by the existence of transfers of information. The directions of these transfers are different in each case: strongly dominant direct transfer for M3, dominant direct transfer for M2, no preferential transfer for Ma, and dominant reverse transfer for Mb. These different behaviors are only partially understood in terms of the characteristic time scales of the model: it seems indeed reasonable to consider that a fast variable F does not influence a slower one S, because its average (taken on a time such that S had not evolved) vanishes, while S influences F because it acts like a drift on F. Nevertheless, this argument leads to the correct conclusion only for M3 and Mb. It is not able to describe the properties of M2 and it does not explain the differences between Ma and Mb. Arguments using the existence of conserved quantities do not seem more useful in this description. Thus the two-time correlations provide original and independent information on the dynamics of the models. Also, it is remarkable that there is a close connection between the direction of the information transfer described by these two-time correlations and the observed curvature of the ξ_n in each model. We have characterized this curvature by its second derivative and we observe that it is negative for M3 (strongly dominant direct information transfer), slightly negative for M2 (slightly dominant direct information transfer), vanishing for Ma (no net information transfer), and slightly positive for Mb (dominant inverse information transfer). It is thus reasonable to conclude that the dominance of reverse versus direct transfer of information is a key phenomenon determining whether the intermittency corrections are convex or concave. It is then interesting to determine how this phenomenon, fully captured by the complex dynamics of shell models, may be accounted for in other approaches.

IV. INFORMATION TRANSFER AND STRUCTURE FUNCTION IN OTHER MODELS

A time-independent model has been proposed to sketch the dynamics generated by the shell model equations [15] for the 3D case. It is assumed that the variable ρ_n is related to ρ_{n-1} by a multiplicative random process given by

$$\rho_n = a_n \rho_{n-1} = C(1 - \mu S_{n-1})\rho_{n-1} \ , \tag{15}$$

where $S_j = \sin(\Delta_j) = \sin(\theta_{j+1} + \theta_j + \theta_{j-1})$. A uniform distribution in $[-\pi, 0]$ is chosen for the independent Δ_j in order to fit the observed S_j distribution. Assuming stationarity, the equations for the moments $\langle U^p \rangle$ lead to

$$\alpha \langle \rho_j^p \rho_{j+1} \rho_{j+2} S_{j+1} \rangle + \beta \langle \rho_j^p \rho_{j-1} \rho_{j+1} S_j \rangle + \gamma \langle \rho_j^p \rho_{j-1} \rho_{j-2} S_{j-1} \rangle = 0 \tag{16}$$

or, using (15) and the definition $\Pi_p = \langle (1 - \mu S_{n-1})^p \rangle$,

$$\alpha C^6 \Pi_{p+2}^2 \Pi_2 (\Pi_1 - \Pi_2) + \beta C^3 \Pi_{p+2} \Pi_{p+1} (\Pi_1 - \Pi_2) + \gamma \Pi_{p+1} (\Pi_p - \Pi_{p+1}) = 0. \tag{17}$$

This set of equations is a recurrence for the Π_n, which, has a solution for M3 when $C^3 \Pi_3 = 1$ (energy constraint) and $\mu \simeq 0.54$. The ξ_n are given by

$$\xi_p = p/3 - \log_g (C^p \Pi_p) \tag{18}$$

and fit the convex deviations from the Kolmogorov scaling law for M3.

This derivation is self-consistent, but relies at the very beginning on the assumption that the information transfer is dominantly forward. Indeed ρ_n is given by (15) so that the amplitude of ρ_{n-1} influences ρ_n. In order to stress the importance of this assumption, we first notice that Eqs. (16) and (17) are invariant if we change $\{\alpha, \rho_j, S_j\}$ into $\{\gamma, \rho_{-j}, S_{-j}\}$. We then introduce the multiplicative random process

$$\rho_j = b_j \rho_{j+1} = C(1 - \mu S_{j+1})\rho_{j+1} \ , \tag{19}$$

which corresponds to a backward transfer of information. The same arguments leading to Eq. (17) now yields

$$\xi_p = p/3 + \log_g (C^p \Pi_p) \ , \tag{20}$$

which is concave. Thus, here again there is a univocal relation between the curvature of ξ_p and the sense of the information transfer.

In fact, this relation is also valid for the simpler approach developed by Paladin and Vulpiani [18], using the Cauchy-Schwarz inequality [19]. Assuming that the random variables δU_n satisfy the scaling laws $\langle |\delta U|^n \rangle = C_n (\frac{l}{l_0})^{\xi_n}$ (l_0 is a characteristic length), the Cauchy-Schwarz inequality implies

$$C_{2n}^2 \left(\frac{l}{l_0} \right)^{2\xi_n} \leq C_{n+h} \left(\frac{l}{l_0} \right)^{\xi_{n+h}} C_{n-h} \left(\frac{l}{l_0} \right)^{\xi_{n-h}} . \tag{21}$$

For large Reynolds numbers, the inertial range is bounded by the large-scale L, where energy is injected. A possible choice for l_0 could then be L, which implies $l < L$ and, in turn,

$$\xi_n \geq \frac{\xi_{n+h} + \xi_{n-h}}{2} + \frac{1}{2} \log_{l/L} \left(\frac{C_{n+h} \, C_{n-h}}{C_n^2} \right) . \tag{22}$$

In the limit $l/L \to 0$, the last term of (22) vanishes

and the convexity of the ξ_p is proven (in agreement with experimental data). However, arguments based on the Cauchy-Schwarz inequality lead to the correct convex ξ_n only because they are combined with the assumption that information is transferred from large to small wavelengths. In that case, it is natural to consider that l_0 is given by the largest length in the system. On the contrary, if information is mainly transferred from small to large wavelengths, it would be more natural to consider that l_0 is the smallest wavelength ℓ in the problem and concave ξ_n would be obtained. When information transfers are direct and reverse, the double limit $L \ll l_0 \ll \ell$ would prove the linearity of ξ_p. The Cauchy-Schwarz inequality is thus compatible with all the behaviors of our shell models.

It appears also that the assumptions made in the random-β model [7] are of the same nature. The convexity of the ξ_n is a consequence of the dependence of the small-scale variables on the large-scale ones, which is equivalent to the introduction of a one-way transfer of information.

In all these cases, the proof of convexity of the ξ_n relies on an implicit assumption of the direction of information transfer, which cannot be derived from mathematical considerations. The introduction of the opposite assumption leads to the proof of the concavity of the ξ_n. This analysis agrees with our conclusion for the shell models.

V. CONCLUSION

We have shown that there is a close connection between the structure function and the information transfer (described by two-time correlations) in a shell model. Four shell models characterized by different conservation properties have been considered. The first one M3, conserving both energy and helicity, is used to model the three-dimensional turbulence. For two-dimensional turbulence, we have studied the model M2 conserving both energy and enstrophy. We have also considered two other test models Ma and Mb, which have special conservation laws that are not related to particular physical systems. In each case, the two-time correlations of the shell variables are obtained by direct simulation of the model.

The simulation of M3 shows a single maximum after a positive delay τ_1 in the correlation between shell variables n and $n+1$. We thus conclude that M3 is characterized by a dominant forward transfer of information, i.e., the variable n is influenced more by the past of shell $n-1$ than by the past of shell $n+1$. Moreover, the cascade processes in M3 seem to be dominated by the transfer between first neighbors. Indeed, the maximal correlation between second (or more distant) neighbors occurs after a delay that is well approximated by the simple addition of the delays needed to reach the maximal correlations between first neighbors. The other models M2, Ma, and Mb show both forward and backward transfers of information and two peaks are observed in the correlation function with, respectively, positive and negative characteristic times. The relative importance of these peaks shows that M2 and Mb are dominated, respectively, by direct and reverse transfers of information. As for Ma, both forward and backward transfers seem to be equivalent.

These properties of the transfer of information have been compared to the ξ_p of the high-order correlation $\langle |U_n|^p \rangle \propto k_n^{\xi_p}$ for each shell model. It appears that the main direction of information transfer seems to determine univocally the characteristics of the intermittency corrections in the ξ_n (convex or concave). More precisely, systems with concave (convex) ξ_n are characterized by dominant backward (forward) information transfers. It is also important to note that this property of the ξ_n cannot be derived so easily from other quantities such as the scaling of characteristic time in each shell or the direction of cascade of the conserved quantities. The same relation between information transfer and the ξ_n can be obtained analytically for other intermittency models such as the multiplicative random process approach by Benzi *et al.* [15], the random-β model [7], or the results derived from the Cauchy-Schwarz inequality [18,19].

The main result of our approach is to provide an original tool to analyze intermittency corrections to Kolmogorov scaling in shell models and in other simple turbulence models. It should be interesting to extend the analysis of two-time correlations to more complex models and even to real turbulence. Experiments [3] have shown that the intermittency corrections are clearly convex in three-dimensional turbulent systems. If our analysis can be extended to real turbulence, it is reasonable to believe that turbulence is characterized by a forward information transfer. This could be of major interest in turbulence modeling. For instance, models for the subgrid scale stress $\tau_{ij} = \overline{u_i u_j} - \bar{u}_i \bar{u}_j$ are needed in large eddy simulation (LES) of complex flows [20]. Here we denote by the overbar the filtering operation that is used to transform the NS equations into the LES equation. Usually, models for the subgrid scale stress τ_{ij}^M are given by some functional of the filtered velocity field taken at the same time: $\tau_{ij}^M(t) = \tau_{ij}^M[\overline{u}_l(t)]$. Our analysis suggests that the small scales evaluated at time t are more strongly correlated with the large scales observed at time $t-\tau$. It would be more natural to propose some subgrid scale model with the property

$$\tau_{ij}^M(t) = \tau_{ij}^M[\overline{u}_l(t-t^*)] \ . \tag{23}$$

The determination of t^* requires a careful analysis of two-time correlations in real turbulence, which is a difficult problem. However, the use of the general formula (23) could improve the accuracy of subgrid scale models for LES. This accuracy is often measured [21] in terms of the correlation between the model τ_{ij}^M and the observed values of the subgrid scale stress $\tau_{ij} = \overline{u_i u_j}$. Thus, by definition of the information transfer, we expect $\tau_{ij}(t)$ to be more strongly correlated with $\tau_{ij}^M[\overline{u}_l(t-t^*)]$ than $\tau_{ij}^M[\overline{u}_l(t)]$.

ACKNOWLEDGMENTS

We are thankful to M. H. Jensen and K. H. Spatschek for their hospitality and for fruitful discussions and to L.

G. Paladin, L. Biferale, A. Vulpiani, R. Grauer, and R. Balescu for interesting discussions. One of us (D.C.) acknowledges financial support from the Fonds National de la Recherche Scientifique (Belgium). Calculations were made on the Cray Y-MP2E-116 computer of the Centre de Calcul of the ULB-VUB. The Service de Physique Statistique is part of the Association EURATOM–Etat Belge.

[1] A.N. Kolmogorov, Dokl. Akad. Nauk SSSR **30**, 299 (1941).
[2] D.R. Chapman, AIAA J. **17**, 1293 (1979).
[3] F. Anselmet, Y. Gagne, E.J. Hopfinger, and R.A. Antonia, J. Fluid Mech. **140**, 63 (1984).
[4] U. Frisch and G. Parisi, in *Turbulence and Predictability in Geophysical Fluid Dynamics and Climate Dynamics*, edited by M. Ghil, R. Benzi, and G. Parisi (North-Holland, Amsterdam, 1985), p. 71.
[5] C. Menneveau and K.R. Sreenivasan, Phys. Rev. Lett. **59**, 1424 (1987).
[6] U. Frisch, P.-L. Sulem, and M. Nelkin, J. Fluid Mech. **87**, 719 (1978).
[7] R. Benzi, G. Paladin, G. Parisi, and A. Vulpiani, J. Phys. A **17**, 3521 (1984).
[8] M.S. Borgas, Phys. Fluids A **4**, 2055 (1992), and references therein.
[9] Z.-S. She and E. Leveque, Phys. Rev. Lett. **72**, 336 (1994).
[10] M. Yamada and K. Ohkitani, Phys. Rev. Lett. **60**, 983 (1988); Prog. Theor. Phys. **79**, 1265 (1988); **81**, 329 (1989); **84**, 415 (1990).
[11] M.H. Jensen, G. Paladin, and A. Vulpiani, Phys. Rev. A **43**, 798 (1991); **45**, 7214 (1992).
[12] J.L. Ottinger and D. Carati, Phys. Rev. E **48**, 2955 (1993).
[13] L. Kadanoff, D. Lohse, J. Wang, and R. Benzi, Phys. Fluids A **7**, 617 (1995).
[14] L. Biferale, A. Lambert, R. Lima, and G. Paladin, Physica D **80**, 105 (1995).
[15] R. Benzi, L. Biferale, and G. Parisi, Physica D **65**, 163 (1993).
[16] E. Aurell, G. Boffetta, P. Frick, G. Paladin, and A. Vulpiani, Phys. Rev. E **50**, 4705 (1994)
[17] R.H. Kraichnan, Phys. Fluids **10**, 1417 (1967); J. Fluid Mech. **47**, 525 (1971).
[18] G. Paladin and A. Vulpiani, Phys. Rep. **156**, 147 (1987).
[19] W. Feller, *An Introduction to Probability Theory and its Application* (Wiley, New York, 1971), Vol. 2.
[20] R. Rogallo and P. Moin, Annu. Rev. Fluid Mech. **16**, 99 (1984).
[21] R. Clark, J. Ferziger, and W. Reynolds, J. Fluid Mech. **91**, 1 (1979).